Applied Water Science (2022) 12:263
https://doi.org/10.1007/s13201-022-01775-4

ORIGINAL ARTICLE

Performance evaluation of amino-functionalized mesoporous/PES nanofiltration membrane in anionic dye removal from aqueous solutions

Mahya Samari[1] · Sirus Zinadini[1,2] · Ali Akbar Zinatizadeh[1,2] · Mohammad Jafarzadeh[3] · Foad Gholami[1]

Received: 15 July 2022 / Accepted: 29 September 2022 / Published online: 2 November 2022

Abstract
In this study, the FSM-16 and FSM-16 modified by metformin (FSM-16-met) additives were applied as modifiers for polyethersulfone-based membranes. The modified membranes were evaluated in terms of morphology, surface roughness, hydrophilicity, pure water flux, pore size and porosity, and resistance ability. The obtained experimental data indicated promising enhancement in permeated flux and hydrophilicity after introducing the FSM-16-met nanomaterials into the membrane texture. In the case assessment of the fabricated membranes, dye removal capability was performed using the direct red-16 and methyl orange (30 mg/L). The modified membranes showed significantly higher dye rejection ability (> 97% for direct red-16 and 95% for methyl orange) compared to the bare membrane (76% for direct red-16 and 74% for methyl orange). The antifouling evaluations were run for milk powder (1000 mg/L) filtration and the best performance was obtained for the modified membrane with 0.1wt.% FSM-16-met (FRR = 95.55 ± 1.91%, R_{ir} = 4.45 ± 0.089%). Also, the effect of the feed pH and concentration, temperature, and membrane driving force was considered on the membrane behavior. High stability in long-term performance was also observed for the modified membrane after 25 h re-running.

Keywords Membrane · Anionic dye removal · Metformin · FSM-16 · Nanofiltration

Introduction

Increased demand for water along with water pollution resulted in an immediate urgent for water reuse (Moradi et al. 2019). Numerous wastewater treatment methods have been developed, such as biochemical, chemical, and physical processes (Yang et al. 2012). Various limitations include complex operating methods, production of harmful by-products, sludge, and environmentally resistant materials are ahead (Baker 2010). Membrane separation processes have emerged as promising technologies for wastewater treatment and water reuse (Moradi et al. 2018; Abdikheibari et al. 2018; Anand et al. 2018). They offer numerous benefits such as cost-effectiveness, being environmentally friendly, excellent efficiency and quality, and easy operation (Wang et al. 2018; Yao et al. 2016; Hegab et al. 2015). Polyethersulfone (PES) has received much attention due to its unique properties, such as mechanical and thermal stability (Bruggen 2009). The fouling phenomenon is one of the main problems of polymeric membranes (Xu et al. 2016). The hydrophobic nature of PES-based membranes is the vulnerability result to fouling, which is due to strong interactions between the membrane surface and foulants, leading to blockage of pores (inner deposition) and outer membrane deposition during the filtration process (Rajabi et al. 2015).

It has been reported in various studies to reduce the aforementioned problems such as plasma treatment, bonding hydrophilic monomers, and combination with hydrophilic additives (Seman et al. 2012; Moghimifar et al. 2015; Ng et al. 2013; Noeiaghaei et al. 2014). Lately, the combination of nanoparticles (NPs) with polymer texture has led to the preparation of mixed matrix membranes (MMM) with increased high selectivity and permeability flux and substantial anti-fouling properties related to increased

✉ Sirus Zinadini
sirus.zeinaddini@gmail.com

[1] Department of Applied Chemistry, Faculty of Chemistry, Razi University, Kermanshah 67144-14971, Iran

[2] Environmental Research Center (ERC), Razi University, Kermanshah, Iran

[3] Department of Organic Chemistry, Faculty of Chemistry, Razi University, Kermanshah 67144-14971, Iran

hydrophilicity and altered membrane morphology (Bano et al. 2015; Kim and Bruggen 2010). Nano-shaped materials (e.g., MWCNT, GO, zeolite, boehmite, Fe_3O_4, TiO_2, ZnO, SiO_2, Fe NPs, and Cu NPs) have been used as modifiers for PES-based membranes (Zinadini et al. 2017; Ghaemi et al. 2015; Vatanpour et al. 2012a; Vatanpour et al. 2012b; Vatanpour et al. 2012c; Qin et al. 2005; Rambabu and Velu 2014; Akar et al. 2013). Moghimifar and coworkers reported the coating of the PES membranes with zeolite and TiO_2 NPs, and the results indicated notable separation performance and anti-fouling behavior with no significant changes in the membrane texture (Moghimifar et al. 2015). Fouled silica mesoporous (FSM-16) are adsorbed, because of pore size distribution, large surface area, and porosity (Samari et al. 2021).

In our previous work, FSM-16 and metformin-modified FSM-16 (FSM-16-met) were used for the fabrication of PES-based ultrafiltration membranes for the separation of oil/water mixture (Samari et al. 2021). The promising performance of the ultrafiltration of PES/FSM-16-met membranes has encouraged us to design nanofiltration membranes based on PES and FSM-16-met for eliminating dyes from wastewater. The fabricated membranes were characterized with SEM and AFM, and their performances were evaluated by measuring zeta potential, contact angle, porosity, and water flux. Organic dyes of direct red-16 (DR-16) and methyl orange (MO) were used in this study.

Material and methods

Materials

Polyethersulfone (MW = 58,000 g.mol^{-1}), dimethylacetamide (DMAc), and polyvinylpyrrolidone (MW = 25,000 g.mol^{-1}) were all supplied from Merck (Germany). All materials were used immediately after receiving, without secondary purification. Distilled water has been used in all experiments.

Modification of nanoparticles

FSM-16 was initially prepared using the reported method (Hashemi-Uderji et al. 2019) and subsequently modified with metformin according to our previous report (Samari et al. 2021). In brief, FSM-16 (1 g) was added to dried toluene (50 mL) containing 3-chloropropyltrimethoxysilane (CPTMS, 0.6 g) and refluxed for 24 h. The resulting powder (i.e., FSM-16-Cl) was separated by centrifugation, washed with dichloromethane and methanol several times, and dried overnight at 80 ℃. A quantity of FSM-16-Cl (1 g) was added to the mixture of metformin (1 g), NaOH (0.25 g), and KI (1 g) in acetonitrile (30 mL), and the mixture was refluxed for 12 h. The synthesized FSM-16-met was centrifuged, washed with ethanol and distilled water, and dried at 80 °C for 24 h.

Fabrication of the membranes

The PES-based membranes were fabricated via the phase inversion method. Table1 shows the constituents of the fabricated membranes. The prepared casting solutions were homogenized by keeping the mixture stirring (400 rpm) overnight and sonication for 20 min to remove all air bubbles. By applying a film applicator(150 µm thickness). membranes were cast on neat glassy plates. The plates were submerged in distilled water to form the flat-sheet membranes. To complete phase separation, after the formation of polymeric membrane, they were transferred to unused distilled water, overnight. Subsequently, the fabricated membranes were dried at room temperature overnight (Samari et al. 2020).

Characterization techniques

The membrane characteristics have been evaluated by various techniques. The scanning electron microscopy was applied to examine the surface morphology (SEM, model: Philips-XL30). The membrane surface roughness was evaluated by atomic force microscopy (AFM, Nanosurf® Mobile). The

Table 1 The composition of the fabricated membranes

Membrane type	PES (wt.%)	PVP (wt.%)	Additive (wt.%)	DMAc (wt.%)
M0	20.0	1.0	0.0	79.0
M1	20.0	1.0	0.1[a]	78.9
M2	20.0	1.0	0.3[a]	78.7
M3	20.0	1.0	0.5[a]	78.5
M4	20.0	1.0	0.1[b]	78.9
M5	20.0	1.0	0.3[b]	78.7
M6	20.0	1.0	0.5[b]	78.5

a: FSM-16, b: FSM-16-met

hydrophilicity of the fabricated membranes was measured by water contact angle (WCA).

Porosity measurements

The gravimetric method was used for determining the membrane porosity (ε). A random portion of the membrane was selected, cut (2×2 cm), and then weighed. The membrane was then submerged in distilled water and weighed again (after 24 h). The membrane porosity can be calculated by Eq. (1):

$$\varepsilon = \frac{\omega_1 - \omega_2}{A \times L \times dW} \tag{1}$$

where ω_1 and ω_2 are the membrane weight after and before immersing in water. A, L, and dW are surface diameter (m^2), thickness, and water density (999 kg. m^3), respectively (Gholami et al. 2018).

Membrane setup and performing analysis

To investigate the membrane performance, a dead-end setup was applied which was made of stainless steel (150 mL, 12.56 cm^2) armed with an N_2 gas (Fig. 1). Three frequent experiments were consecutively examined (distilled water-feed-distilled water) (simulated dye feed (30 ppm, DR-16, and MO) and 1000 ppm milk powder solution as fouling agents were applied as feed). Firstly, distilled water was filtered (60 min), then without any further operation, milk powder (1000 ppm) or dye feed was passed (90 min) and the membrane was washed with distilled water, after this step, distilled water was finally filtered again (60 min). The PWF was calculated by Eq. (2):

$$J_{w.1} = \frac{M}{A\Delta t} \tag{2}$$

where $J_{W.1}$, M, A, Δ t, are PWF ($kg/m^2.h$), the weight of permeated volume (kg), membrane surface area (m^2), and filtering time (h), respectively.

Fig. 1 The image of the applied membrane setup

For evaluation of the membrane recovery, membrane flux recovery ratio (FRR) was determined using the experimental data of fouling solution filtration (milk powder) (Eq. 3):

$$FRR = \left(\frac{J_{w.2}}{J_{w.1}}\right) \times 100 \tag{3}$$

here $J_{W.2}$, and $J_{W.1}$ are the permeated volume ($kg/m^2.h$) after and before the milk powder filtering. The membrane fouling resistance including irreversible resistance (R_{ir}), reversible resistance (R_r), and total resistance (R_t) were evaluated according to Eqs. 4, 5, and 6:

$$R_t(\%) = \left(1 - \frac{j_p}{j_{w.1}}\right) \times 100 \tag{4}$$

$$R_r(\%) = \left(\frac{j_{w.2} - j_p}{j_{w.1}}\right) \times 100 \tag{5}$$

$$R_{ir}(\%) = \left(\frac{j_{w.1} - j_{w.2}}{j_{w.1}}\right) \times 100 = R_t - R_r \tag{6}$$

Membrane stability

The mechanical and thermal stabilities of the fabricated membranes were investigated by applying different transmembrane pressures (3, 4, 5, and 6 bar) and different thermal conditions (30, 45, 60, and 75 ºC).

Rejection

A spectrophotometer was applied to evaluate the membrane ability for dye rejection of DR-16 ($\lambda = 526$ nm) and MO ($\lambda = 464$ nm) by the following equation:

$$R\% = \left(1 - \frac{C_P}{C_F}\right) \times 100 \tag{7}$$

where C_F and,C_P are the dye concentrations of the feed and permeate solutions.

Moreover, the rejection performance of the optimally modified membranes (M1 and M4) was compared with that of the bare membrane at different pHs. The long-term durability of the fabricated membranes in the filtration process was also examined.

Results and discussion

Physico-chemical properties and PWF of membranes

The applied membrane modifiers were synthesized and characterized according to our previously published report (Samari et al. 2021). The bare PES membrane exhibited a hydrophobic nature (Table 2, water contact angle = 98°). Although the WCA of M1 and M4 membranes decreased by increasing the content of FSM-16 and FSM-16-met in the membrane matrix, which indicates the hydrophilic nature of FSM-16-met. In the best case, the WCA of M4 was close to 40.78°, which was notably lower than the other fabricated membranes in this study. The hydrophilicity can be improved by the introduction of active sites ($–NH_2$ and –OH) presenting in FSM-16-met, into the membrane matrix. Additionally, the effect of FSM-16-met on hydrophilicity enhancement can be related to the reduction in interfacial energy (Celik et al. 2011). However, further addition of FSM-16-met into the membrane matrix did not increase the membrane surface hydrophilicity, but rather reduces it to some extent. This could be related to two main reasons: (i) pore size reduction on the surface due to FSM-16-met aggregation in the membrane matrix, and (ii) the reduction of functional groups on the membrane surface. The FSM-16-met has a high tendency to accumulate in high concentrations, leading to a decrease in the effective loading of FSM-16-met into the polymeric matrix.

Table 2 The porosity, mean pore radius, and water contact angle of the fabricated nanofiltration membranes

Membrane type	Porosity (%)	Mean pore radius (nm)	WCA, °
M0	45.76 (±1.3)	5.0 (±0.15)	78.98
M1	69.47 (±2.1)	3.6 (±0.11)	67.58
M2	47.93 (±1.4)	4.0 (±0.12)	70.45
M3	57.26 (±1.7)	4.6 (±0.14)	72.65
M4	80.26 (±2.4)	1.9 (±0.05)	40.78
M5	79.74 (±2.4)	2.2 (±0.07)	52.36
M6	72.9 (±2.2)	2.0 (±0.06)	61.45

The PWF of the fabricated membranes with different contents of unmodified and modified additives are compared in Fig. 2. As anticipated, the PWF increment coincided and was well-matched with an increase in hydrophilicity. The bare PES showed the lowest amount of PWF compared to M1 and M4 membranes. It seems that the increase in porosity, hydrophilicity and the pores size of the M1 and M4 membrane has enhanced the PWF. By adding 0.1 wt.% of FSM-16-met (M4), the PWF was increased to 55.56 kg/m^2. The PWFs of 52.54 and 39.78 kg/m^2 were found for M5 and M6, respectively. The reduction in the PWF with increasing the nanofiller content (> 0.1 wt.%) was related to the increased viscosity of the casting solution, which caused slow phase inversion. In other words, the high loading of nanofiller blocks membrane pores and reduces their mean pore sizes (Zinadini et al. 2014a). The mean pore radius and total porosity of the membranes are given in Table 2. The mean radius and porosity of membranes increased with the addition of FSM-16 up to 0.1 wt.% and then reduced. Dadari

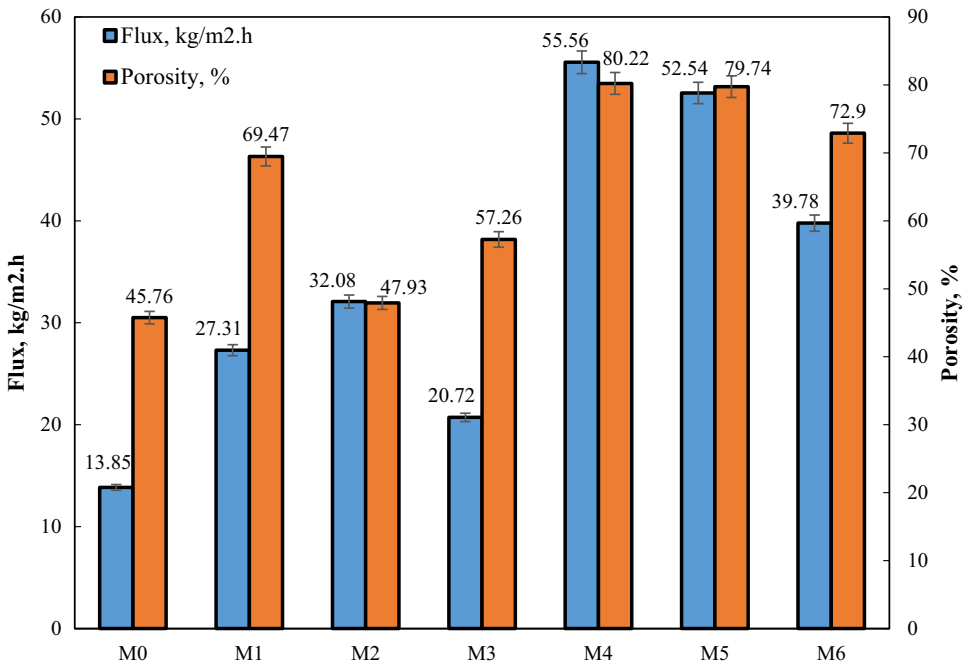

Fig. 2 PWF and porosity of the fabricated membranes

et al. reported a similar behavior for PWF of PES-based nanofilter membrane with embedded adipate-ferro NPs. By increasing FSM-16-met loading to the membrane matrix, the hydrophilicity was improved (Zinadini et al. 2014b). It can be the reason for increasing the pore channel size, porosity, (Table. 2), and PWF (Fig. 2) of the prepared membranes.

The obtained results were proved by SEM (Fig. 3). The modified membranes exhibited relatively smooth structures. The addition of a high amount of FSM-16-met into the polymeric matrix (>0.1 wt.%), hurts the membrane properties. In addition, the effect of compaction was evaluated and the PWF was examined at different transmembrane pressures. Figure 2 shows that by increasing the transmembrane pressure, the PWF was increased and a linear relationship between PWF and pressure was observed. Furthermore, the stability of membranes at harsh thermal conditions (45, 60, 75, and 90 °C) was evaluated (Fig. 4). The results indicated that the thermal stability of the membranes can be enhanced by increasing the additive loading (Samari et al. 2020; Matsumoto et al. 2002).

To realize the effect of additives on the surface roughness of the membranes, the technique of AFM was utilized. The results of surface parameter and topography are presented in Table 3 and Fig. 5, respectively. It was found that the surface roughness of the modified membranes was significantly reduced by the addition of the additive. The bare membrane (M0) exhibited the highest roughness of 45.85 ± 0.97 nm, while the roughness of 1.63 ± 0.05 nm and 1.34 ± 0.04 nm were found for M1 and M4, respectively. This behavior can be related to the regular decoration of additives, in low

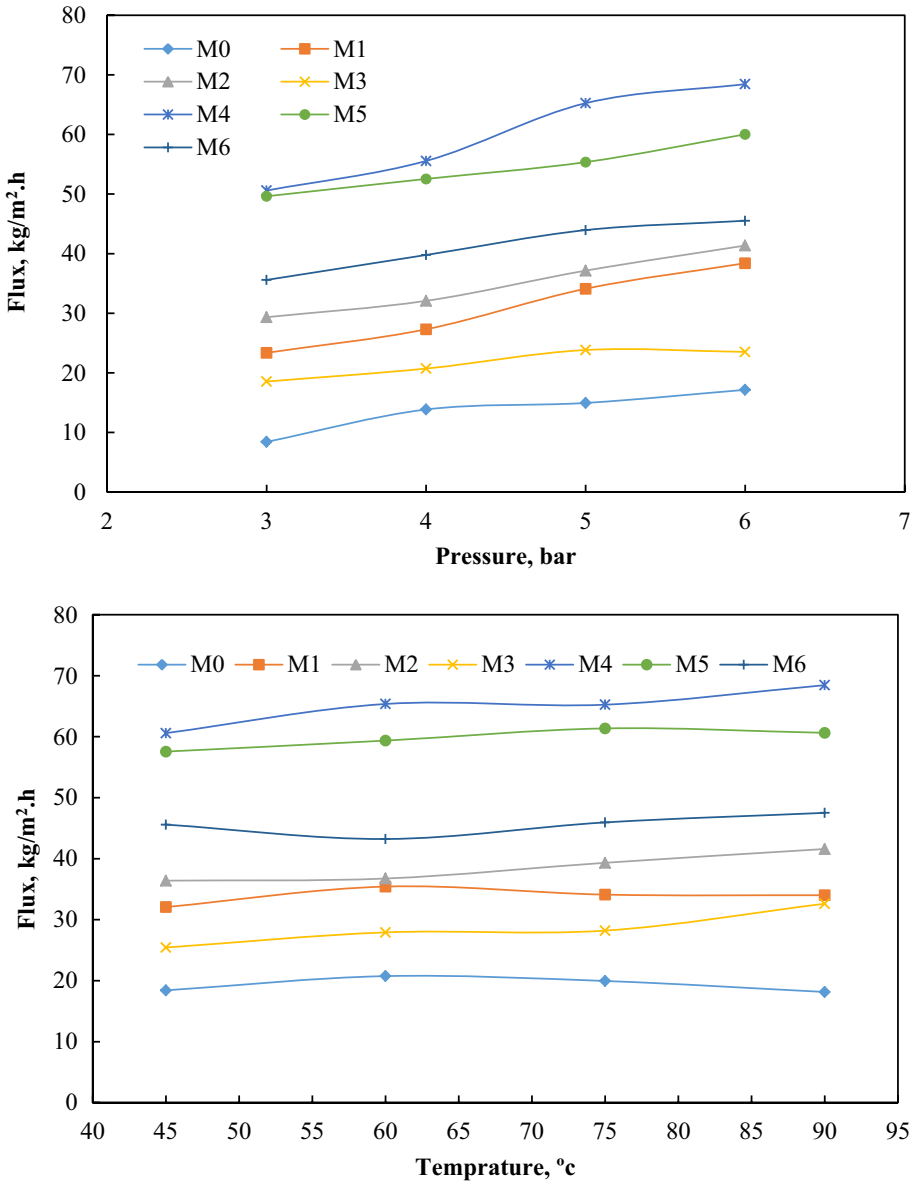

Fig. 3 Cross-sectional SEM images of the fabricated membranes

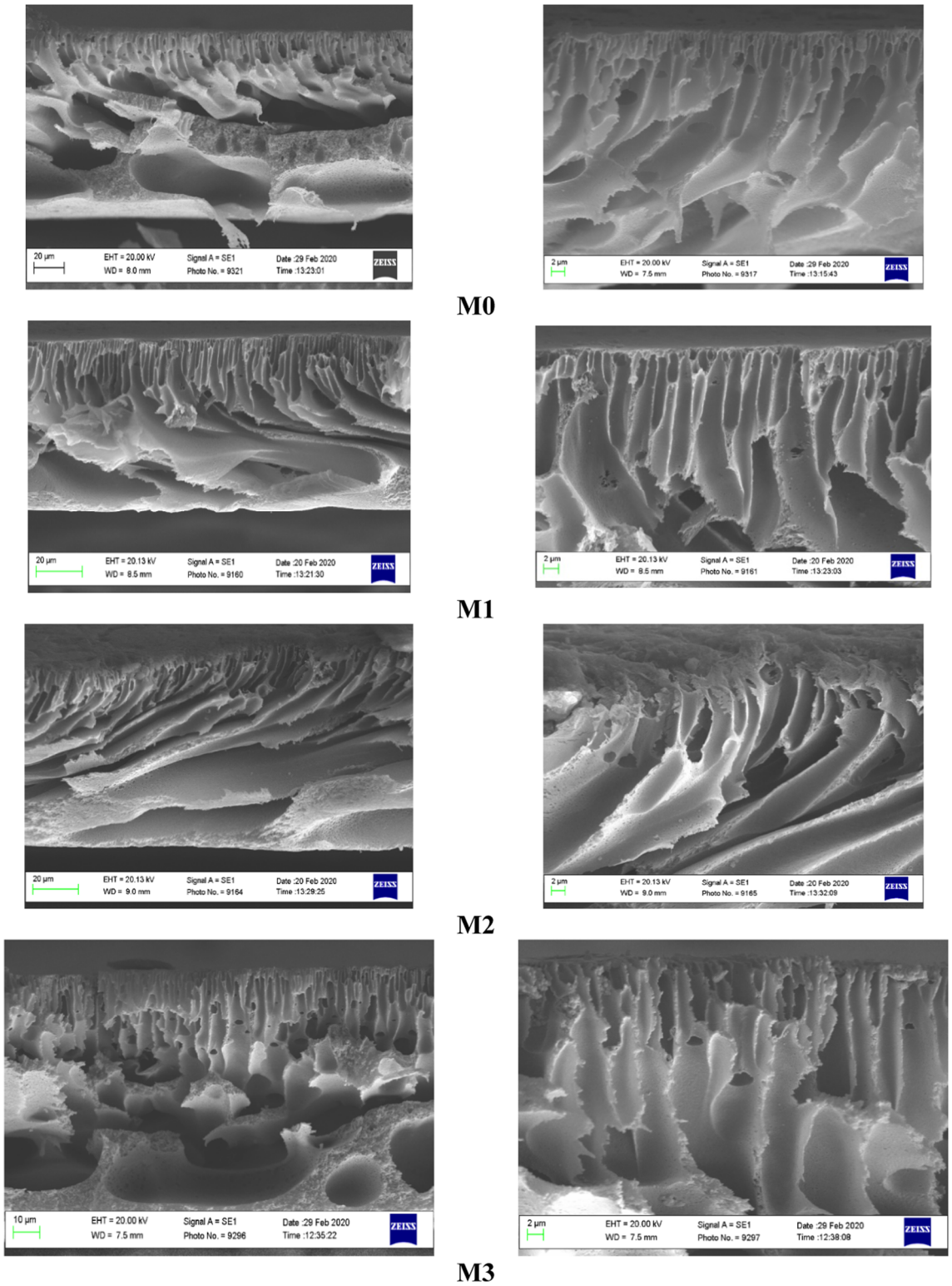

Fig. 4 The effect of transmembrane pressure and temperature on the PWF of the fabricated membranes

content, in the membrane texture, and its lower electrostatic interactions (Rambabu et al. 2019). With increasing the content of additives (> 0.1 wt.%, M3 and M6), the surface roughness was increased due to further accumulation of nanomaterials in the membrane matrix. A similar trend has been observed for graphene oxide (Gholami et al. 2017),

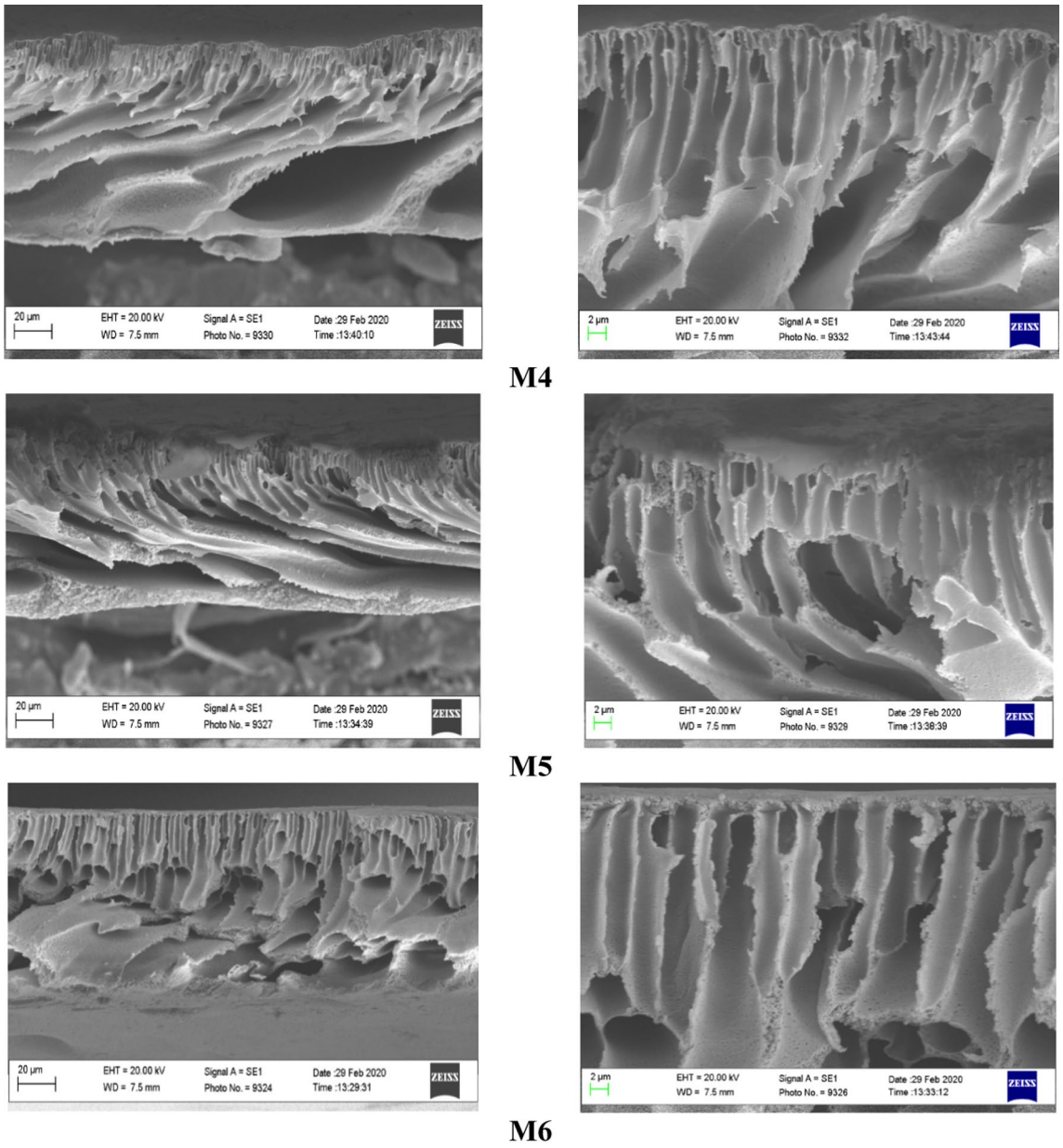

Fig. 4 (continued)

Table 3 The data of surface parameters in the fabricated membranes

S_z (nm)	S_q (nm)	S_a (nm)	Membrane type
112.310	47.190	46.855	M0
36.005	2.183	1.629	M1
64.804	5.018	2.627	M2
59.695	10.645	8.616	M3
22.589	1.811	1.338	M4
44.779	3.592	2.443	M5
13.285	7.724	6.696	M6

Ce-based metal–organic framework (Mohammadnezhad et al. 2019), and isocyanate-treated graphene oxide (Zhao et al. 2013).

Antifouling evaluation

The anti-fouling properties of the membranes were examined by measuring irreversible (R_{ir}), reversible (R_r), total membrane resistance (R_t), and FRR (Fig. 6). The R_t can be divided into R_r and R_{ir}. Higher FRR and lower R_t indicate superior membrane anti-fouling properties. The deposited foulant can be also removed by hydraulic cleaning. The bare

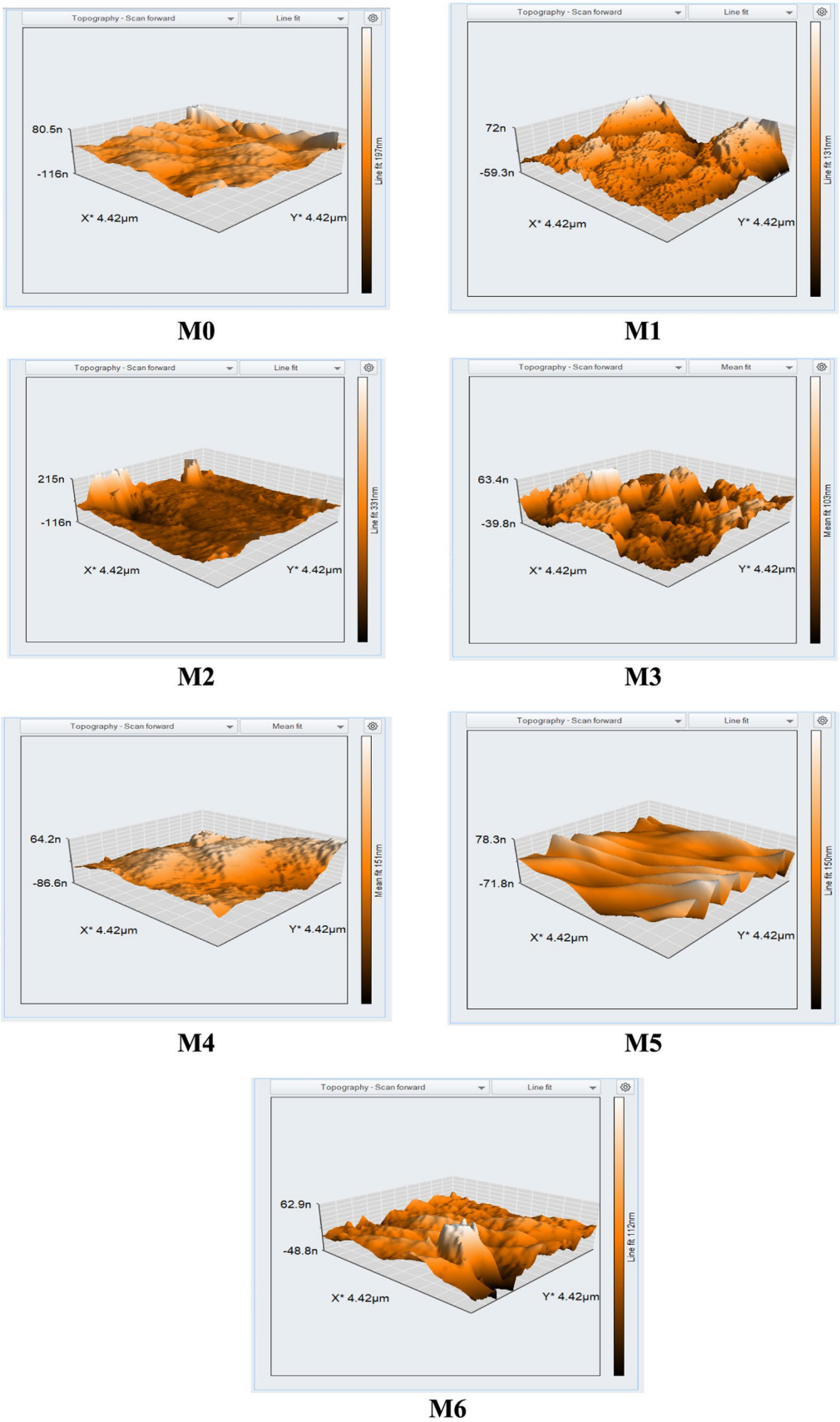

Fig. 5 AFM topographies of the fabricated membranes

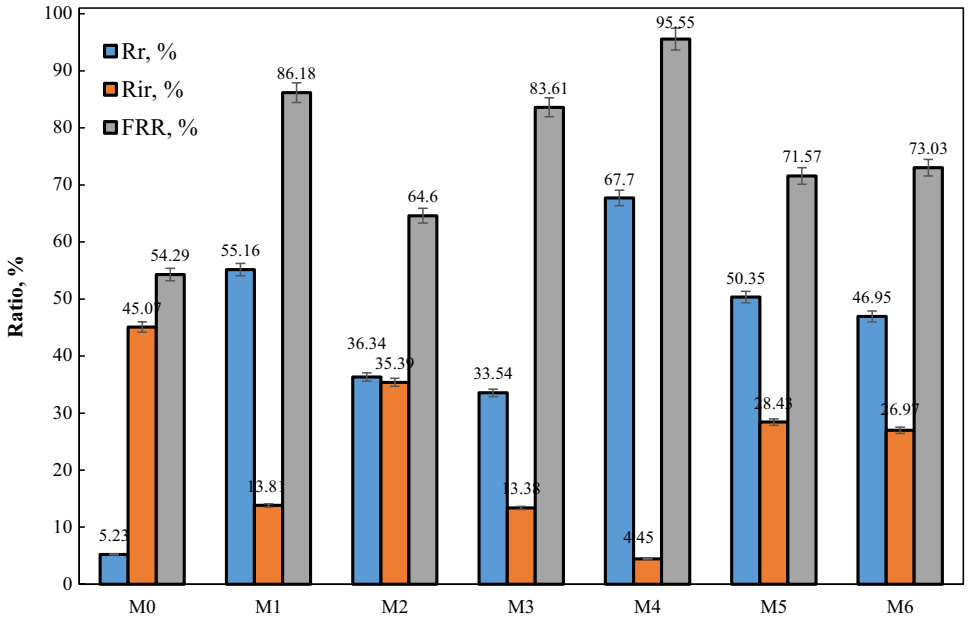

Fig. 6 The FRR, R_r, and R_{ir} of the membranes

membrane (M0) exhibited the highest R_{ir} (45.07%) due to its poor hydrophilicity. By introducing 0.1 wt.% of additives, the corresponding R_{ir} was reduced to 13.1% and 4.45% for M1 and M4, respectively. The best result was observed for the membrane with a modified additive, which could be promising compared to the reported data in the literature (Hashemi-Uderji et al. 2019).

The addition of additives (0.1 wt.%), the corresponding R_{ir}, was reduced to 13.1% and 4.45% for M1 and M4, respectively. The best result was observed for the membrane with a modified additive, which could be promising compared to the reported data in the literature (Samari et al. 2020).

The durability of the membranes was evaluated by three filtration cycles using milk powder solution as a model foulant solution (Fig. 7). For the purification cycle, the FRR of 54.29% was found for M0 due to its hydrophobic nature, while the corresponding values of 86.18 and 95.55% were observed for M1 and M4, respectively. In fact, the membrane with FSM-16-met (M4) exhibited the best recovery performance and the foulants can be easily removed from the membrane surface by physical washing. However, by increasing the additive loading (0.3 and 0.5 wt.%), the corresponding FRR was reduced, which could be related to the enhanced roughness in higher loading.

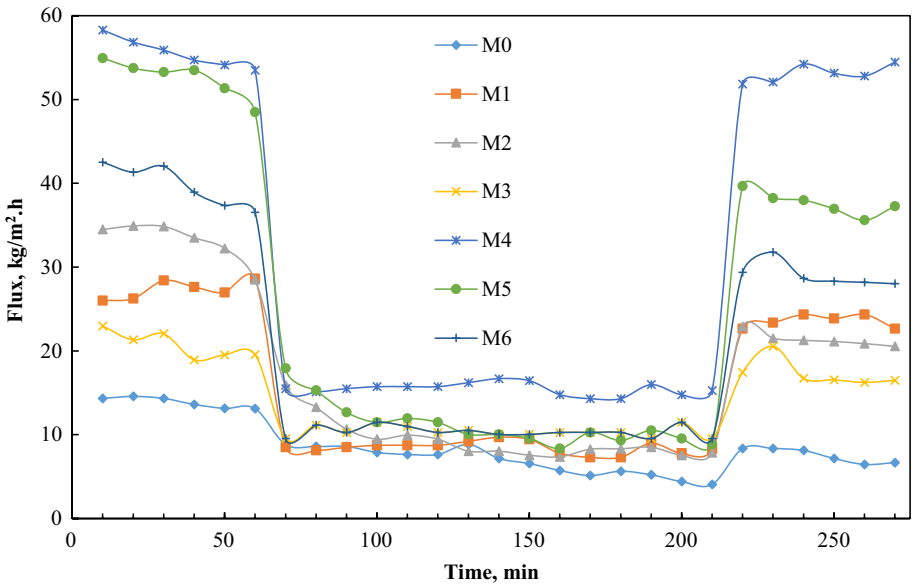

Fig. 7 Fouling behavior for the membranes

Dye rejection

To further justify the widespread application of the fabricated nanofiltration membranes, dye rejection behavior was examined using MO and DR-16 solutions (30 ppm). Table 4 represents the results of dye rejection of various fabricated membranes. The results showed that the modified membranes exhibited higher dye rejection than the bare membrane. It was also found that the surface modification of the additive had a significant effect on the performance of the membranes with modified FSM (i.e., FSM-16-met) compared to using unmodified FSM. The highest dye rejection was found for membrane M4 with 97.5% and 95.5% for DR-16 and MO, respectively. The surface modification of FSM-16 with organic species possessing amine groups ($–NH_2$ and –OH) enhanced the surface hydrophilicity and generated more adsorption sites, which could be beneficial for dye rejection. The data of WCA (Table 2) and zeta potential (Fig. 8) are proved changes in the surface hydrophilicity of membranes with the addition of the additives, particularly modified additives. According to the results of zeta-potential, membrane M4 (PES/FSM-16-met) has negative surface charges at pH = 6 because of the presence of added functional groups located in the pores and membrane texture (Abdi et al. 2018). On the other hand, MO and DR-16 have negative charges in neutral pH due to the dissociation of sulfuric groups; therefore, electrostatic repulsions between the membrane surface and the dyes caused high rejection. In addition, the activated sites in DR-16 (e.g., –NH, –OH, aromatic rings) and/or MO ($–SO_3$, aromatic rings) may form some hydrogen bonding interactions with available functional groups of FSM-16-met ($–NH_2$ and –OH). In fact, the organic dye cannot stabilize on the surface of the modified membrane, PES/FSM-16-met (Fig. 9).

The effect of concentration

In this part of the study, the bare (M0), and optimally modified membranes (M1, and M4) were examined by mixed solutions made of different dyes (DR-16 and MO) in various concentrations (Fig. 10).

As can be seen from the data (a, b) by increasing the dye concentration, the membrane PWF was generally decreased although the dye rejection was kept stable.

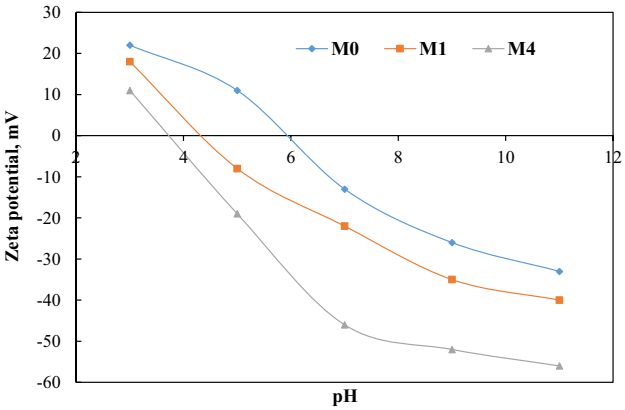

Fig. 8 The zeta potential of the fabricated membranes

According to the obtained data in Fig. 10 (a), dye concentration increment leads to a reduction in membrane rejection. The possible explanation of this phenomenon can be related to the aggregation of the dye molecules in the feed, which could be suppressed by the TDS. In this case, more dye molecules will adsorb in pores and on the membrane surface and form a fouling layer, which acts as an additional resistance layer gradually resulting in a reduction in the effective pore size and then the membrane permeability. When the concentration of dyes was increased from 10 mg/L to 50 mg/L, the rejection essentially changed, and the PWF was dropped (Tavangar et al. 2020; Vatanpour et al. 2020).

The effect of transmembrane pressure

Figure 11 illustrates that, by increasing the transmembrane pressure (TMP), the PWF of bare and optimally modified membranes was increased almost linearly. As can be obtained, the PWF of the optimally modified membrane (M4) was almost 27 kg/m^2.h, at 7 bar pressure while the bare PES exhibits a flux of 18.2 kg/m^2.h at the same pressure for MO dye filtration. The observed linear dependence of PWF on TMP illustrates the stable membrane structure due to the high network crosslinking of the PES membrane. As mentioned before the mean pore size of the modified membrane was increased, which plays a crucial role in PWF enhancement and dye rejection. This phenomenon is likely

Table 4 The data of dye rejection by the membranes

	M0	M1	M2	M3	M4	M5	M6
Direct red-16 (DR-16) rejection, %	76.78	84.41	81.02	83.32	97.54	94.77	95.51
Methyl orange (MO) rejection,%	74.65	83.02	79.25	80.24	95.5	92.96	93.8

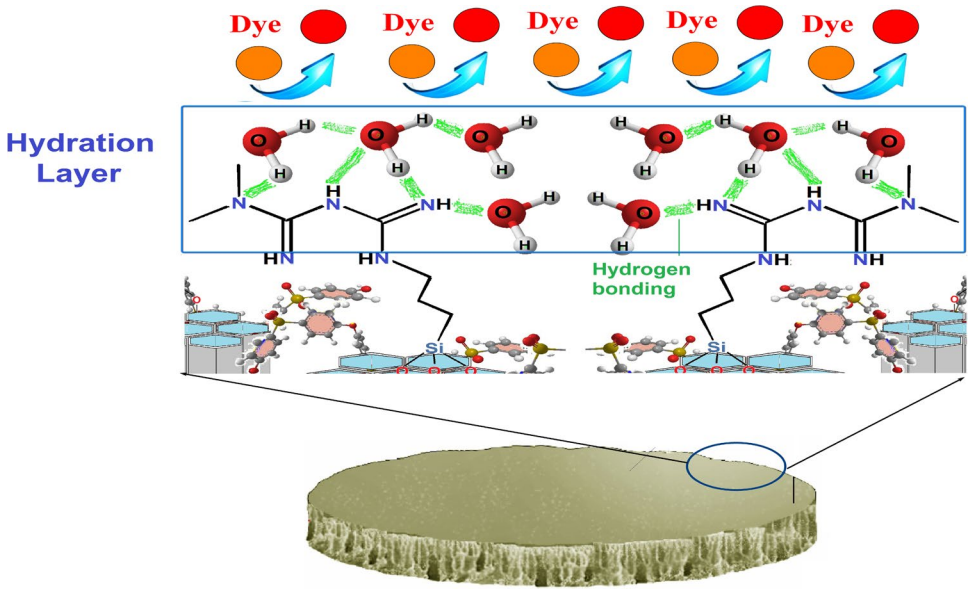

Fig. 9 Interaction between dye molecules and metformin groups on the membrane surface

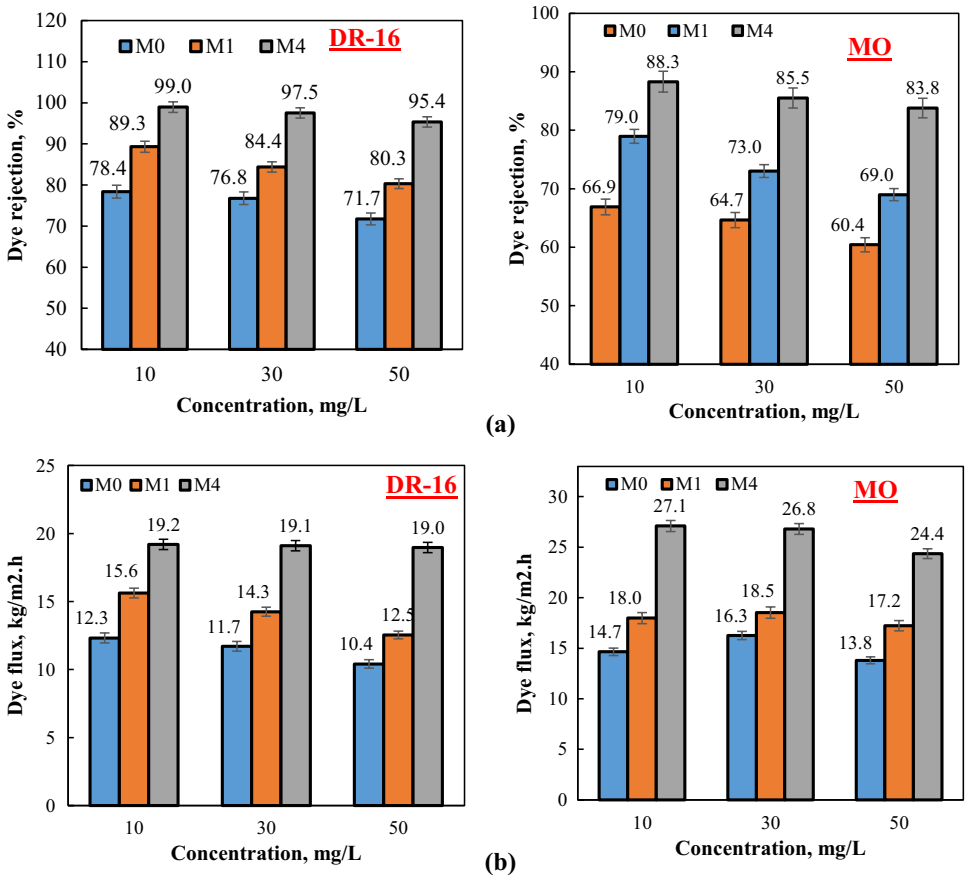

Fig. 10 Dye rejection efficiency (**a**) and dye flux (**b**) of the membranes in different concentrations

following the synergy effect of reduced crosslinking density and loos of microstructure brought by membrane modification (Samari et al. 2021).

The effect of pH

The effect of feed pH on the dye rejection performance of the membranes was investigated at three different pHs (2, 7, 12). According to the presented results in Fig. 12a, the dye

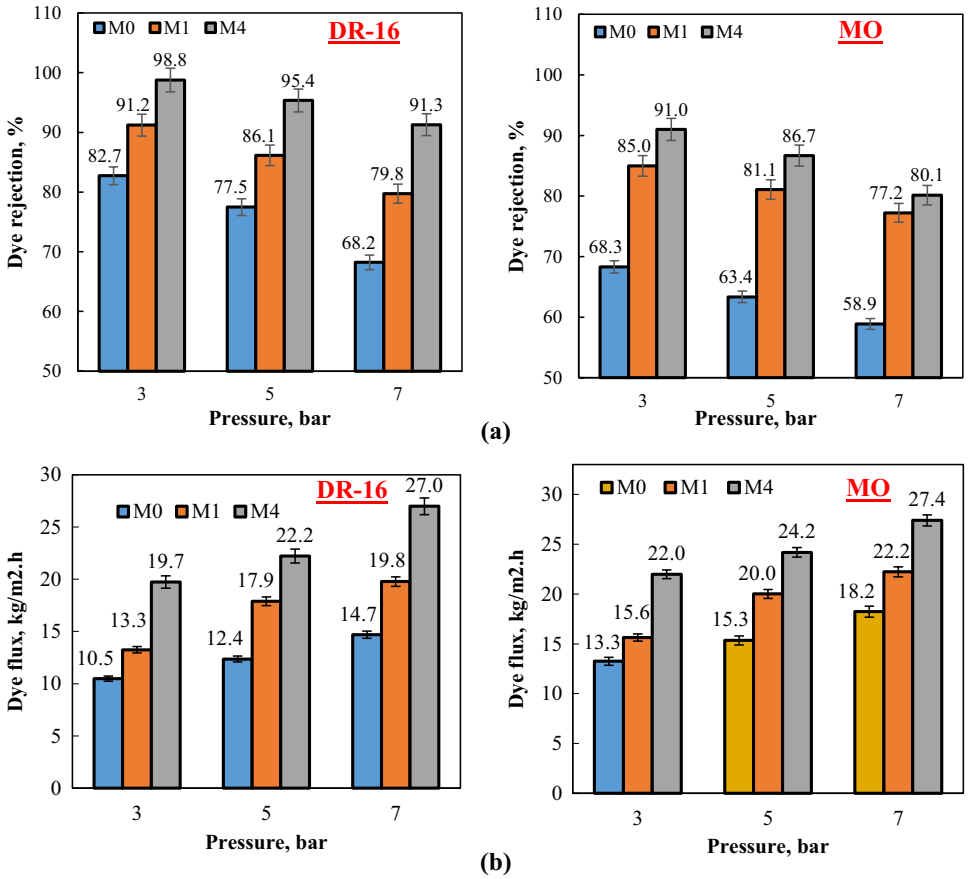

Fig. 11 Dye rejection efficiency (**a**) and dye flux (**b**) of the membranes in different pressure

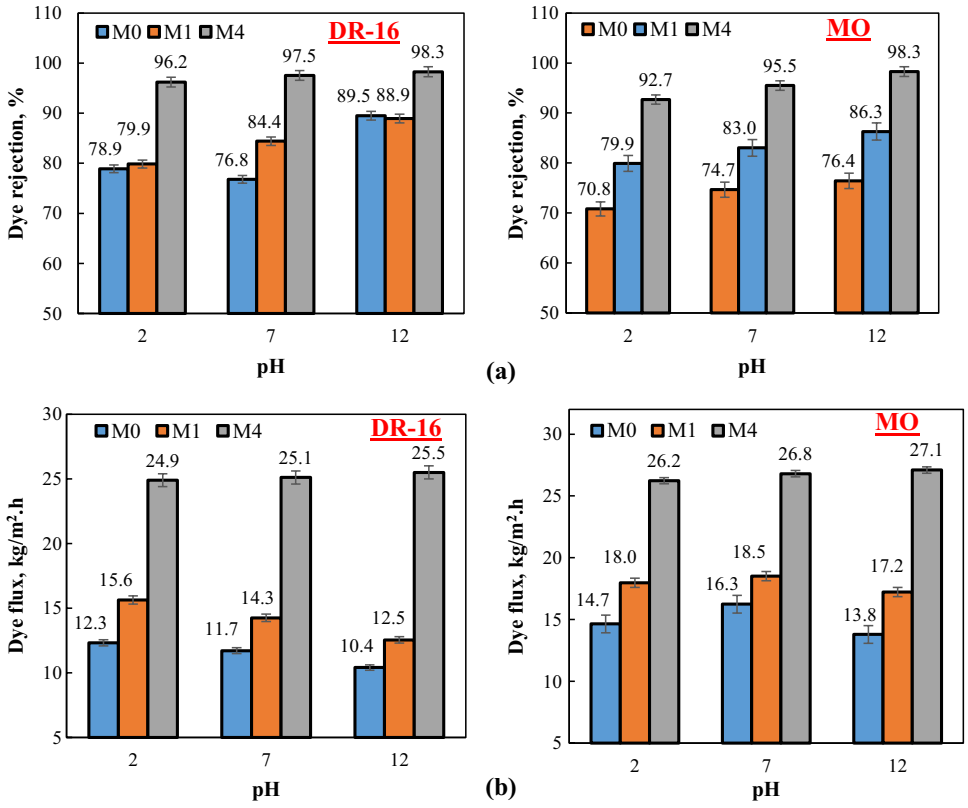

Fig. 12 Dye rejection efficiency (**a**) and dye flux (**b**) of the membranes in different pHs

rejection efficiencies of 70.8, 79.9, and 92.7 were found for M0, M1, and M4 membranes, respectively at acidic pH for MO, compared to the corresponding efficiencies of 78.9, 79.8, and 96.2 for M0, M1, and M4, respectively for DR-16. At pH = 2, the dye molecules turn to acidic form and functional groups (-NH_2) of FSM-16-met protonate rapidly to ammonium (-NH_3^+) groups. Therefore, the electrostatic repulsion between the membrane surface and the feeds enhanced the dye rejection (Moradi et al. 2020). In alkaline conditions (pH = 12), the dye rejection efficiencies were further increased compared to the corresponding in acidic conditions, which could be related to the role of hydrogen bonding in the process of dye rejection. Metformin in FSM-16-met is in bidentate forms in alkaline pH, which facilitates the availability of amine groups. The dye rejection behavior of the membranes is strongly supported by the result of PWF (Fig. 12b). For the M4 membrane, the PWF was higher for DR-16 (25.5 kg/m^2) at pH = 12, due to the fluid volume and enhanced membrane rejection. Similar results were also observed for MO. The best performance was observed for the M4 membrane with an optimal loading of 0.1 wt.% of the modified FSM-16.

Long-term performance

The long-term performance of the membranes was evaluated in nine frequent cycles of the dyes at 30 ppm (Fig. 13). The modified membranes (M1 and M4) exhibited considerable performance and stability within 1500 min compared to the bare membrane. M0 has lost its performance by a significant reduction in PWF (from 14.33 to 0 kg/m^2) after 420 min. This phenomenon displays the effective role of additives in manipulating the texture of polymeric membranes. Furthermore, the enhanced PWF might be related to the generated thin hydration layer on the membrane surface through hydrogen bonding interactions of H_2O molecules with the membrane surface. In other words, by increasing the resistance against the formation of the cake layer on the membrane surface, this phenomenon is pronounced in long-term performance (Fig. 13) (Samari et al. 2020).

The performance of the M4 membrane (PES/FSM-16-met) in dye rejection is compared with other systems reported in the literature (Table 5). Our system exhibited a quite high flux and comparable rejection efficiency in comparison with the reported systems.

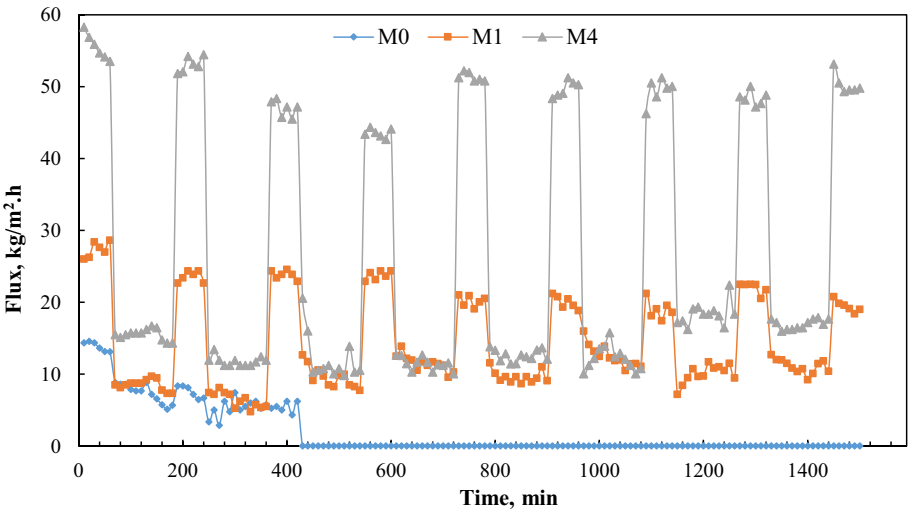

Fig. 13 Long-term performance for the bare (M0) and the optimally modified membranes (M1 and M4) in a dead-end setup

Table 5 A comparison study on the performance of different membranes in dye rejection

Polymer	Membrane	Nanofiller	Flux (kg/m^2.h)	Dye	Rejection, %	Ref
PES	NF	Graphene oxide	20.4 (4 bar)	Direct red-16	99.00	Zinadini et al. 2014a)
PES	NF	TiO_2	32.5 (3 bar)	RB-21	73.01	Safarpour et al. 2016)
PS	NF	Sulfated-TiO_2	6.37 (6 bar)	MB	90.4	Pereira et al. 2015)
PVDF	NF	Halloysite nanotubes	42 (3 bar)	DR-28	94.9	Zeng et al. 2016)
PES	NF	Graphene oxide	13 (1 bar)	Sunset yellow acridine orange	84.9 48.4	Abdel-Karim et al. 2018)
PES	NF	UiO-66-NH_2	–	Congo red Orange II Crystal violet Methylene blue	97.00 83.34 67.1 62.3	Rambabu et al. 2019)
PES	NF	FSM-16-met	55.56 (4 bar)	DR-16 MO	97.5 95.5	This study

Conclusion

In this work, FSM-16 and FSM-16 modified with metformin (FSM-16-met) were utilized as additives to improve the performance of PES-based membrane in the separation of organic dyes from wastewater. PWF, antifouling behavior, and dye rejection efficiency of the membranes were evaluated for the model dyes of MO and DR-16. The results revealed membranes with modified additives showed higher performance than those with unmodified additives. Moreover, higher performances were observed for membranes with low additive loading (0.1 wt.%) compared to membranes with the loading of 0.3 and 0.5 wt.%. The best result was found for a membrane with 0.1 wt.% of FSM-16-met: PWF (55.56 ± 1.11 kg/m^2.h) and rejection efficiency (97.5% and 95.5% for DR-16 and MO, respectively). The antifouling results exhibited that by the introduction of the modified additives to the membrane, the FRR was significantly increased (from 54.29% to 95.55%) compared to the bare membrane, while the irreversible fouling was decreased (from 45.07% to 4.45%) due to enhanced hydrophilicity of the membrane in the presence of the modified additive. Moreover, the results of long-term performance revealed the high stability of the modified membrane. These results can be promising to extend the application of PES/FSM-16-met membrane for purification of industrial wastewater before discharging to the environment and separation of organic pollutants from urban wastewater.

Funding Mahya Samari received no specific funding for this work. Sirus Zinadini received no specific funding for this work. Ali Akbar Zinatizadeh received no specific funding for this work. Mohammad Jafarzadeh received no specific funding for this work. Foad Gholami received no specific funding for this work.

Declarations

Conflict of interest The authors declare that they have no known competing financial interests or personal relationships that could have appeared to influence the work reported in this paper.

5. References

Abdel-Karim A et al (2018) High flux and fouling resistant flat sheet polyethersulfone membranes incorporated with graphene oxide for ultrafiltration applications. Chem Eng J 334:789–799

Abdi G et al (2018) Removal of dye and heavy metal ion using a novel synthetic polyethersulfone nanofiltration membrane modified by magnetic graphene oxide/metformin hybrid. J Membr Sci 552:326–335

Abdikheibari S et al (2018) Thin film nanocomposite nanofiltration membranes from amine functionalized-boron nitride/polypiperazine amide with enhanced flux and fouling resistance. J Mater Chem A 6(25):12066–12081

Akar N et al (2013) Investigation of characterization and biofouling properties of PES membrane containing selenium and copper nanoparticles. J Membr Sci 437:216–226

Anand A et al (2018) Graphene-based nanofiltration membranes for improving salt rejection, water flux and antifouling–a review. Desalination 429:119–133

Baker RW (2010) Research needs in the membrane separation industry: looking back, looking forward. J Membr Sci 362(1–2):134–136

Bano S et al (2015) Graphene oxide modified polyamide nanofiltration membrane with improved flux and antifouling properties. J Mater Chem A 3(5):2065–2071

Van der Bruggen B (2009) Chemical modification of polyethersulfone nanofiltration membranes: a review. J Appl Polym Sci 114(1):630–642

Celik E, Liu L, Choi H (2011) Protein fouling behavior of carbon nanotube/polyethersulfone composite membranes during water filtration. Water Res 45(16):5287–5294. https://doi.org/10.1016/j.watres.2011.07.036

Ghaemi N et al (2015) Polyethersulfone membrane enhanced with iron oxide nanoparticles for copper removal from water: Application of new functionalized Fe3O4 nanoparticles. Chem Eng J 263:101–112

Gholami F et al (2017) Preparation and characterization of an antifouling polyethersulfone nanofiltration membrane blended with graphene oxide/ag nanoparticles. Int J Eng 30(10):1425–1433

Gholami F et al (2018) TMU-5 metal-organic frameworks (MOFs) as a novel nanofiller for flux increment and fouling mitigation in PES ultrafiltration membrane. Sep Purif Technol 194:272–280

Hashemi-Uderji S, Abdollahi-Alibeik M, Ranjbar-Karimi R (2019) Fe3O4@ FSM-16-SO3H as a novel magnetically recoverable nanostructured catalyst: preparation, characterization and catalytic application. J Porous Mater 26(2):467–480

Hegab HM et al (2015) Fine-tuning the surface of forward osmosis membranes via grafting graphene oxide: performance patterns and biofouling propensity. ACS Appl Mater Interface 7(32):18004–18016

Kim J, Van der Bruggen B (2010) The use of nanoparticles in polymeric and ceramic membrane structures: review of manufacturing procedures and performance improvement for water treatment. Environ Pollut 158(7):2335–2349

Matsumoto A et al (2002) Thermal stability and hydrophobicity of mesoporous silica FSM-16. Colloids Surf, A 203(1–3):185–193

Moghimifar V et al (2015) Enhancing the antifouling property of polyethersulfone ultrafiltration membranes using NaX zeolite and titanium oxide nanoparticles. RSC Adv 5(69):55964–55976

Mohammadnezhad F, Feyzi M, Zinadini S (2019) A novel Ce-MOF/PES mixed matrix membrane; synthesis, characterization and antifouling evaluation. J Ind Eng Chem 71:99–111

Moradi G et al (2018) Fabrication of high flux and antifouling mixed matrix fumarate-alumoxane/PAN membranes via electrospinning

for application in membrane bioreactors. Appl Surf Sci 427:830–842
Moradi G et al (2019) Polycitrate-para-aminobenzoate alumoxane nanoparticles as a novel nanofiller for enhancement performance of electrospun PAN membranes. Sep Purif Technol 213:224–234
Moradi G, Zinadini S, Rajabi L (2020) Development of high flux nanofiltration membrane using para-amino benzoate ferroxane nanoparticle for enhanced antifouling behavior and dye removal. Process Saf Environ Prot 144:65–78
Ng LY et al (2013) Polymeric membranes incorporated with metal/metal oxide nanoparticles: a comprehensive review. Desalination 308:15–33
Noeiaghaei T, Kim J-O, Chae S-R (2014) Recent advances in nano-hybrid membranes for advanced water treatment. Curr Org Chem 18(18):2381–2404
Pereira VR et al (2015) Preparation and performance studies of polysulfone-sulfated nano-titania (S-TiO 2) nanofiltration membranes for dye removal. RSC Adv 5(66):53874–53885
Qin J-J, Oo MH, Li Y (2005) Hollow fiber ultrafiltration membranes with enhanced flux for humic acid removal. J Membr Sci 247(1–2):119–125
Rajabi H et al (2015) Nano-ZnO embedded mixed matrix polyethersulfone (PES) membrane: influence of nanofiller shape on characterization and fouling resistance. Appl Surf Sci 349:66–77
Rambabu K, Velu S (2014) Iron nanoparticles blended polyethersulfone ultrafiltration membranes for enhanced metal ion removal in wastewater treatment. Int J Chem Tech Res 6(10):4468–4470
Rambabu K et al (2019) Effective treatment of dye polluted wastewater using nanoporous CaCl2 modified polyethersulfone membrane. Process Saf Environ Prot 124:266–278
Safarpour M, Vatanpour V, Khataee A (2016) Preparation and characterization of graphene oxide/TiO2 blended PES nanofiltration membrane with improved antifouling and separation performance. Desalination 393:65–78
Samari M et al (2020) Designing of a novel polyethersulfone (PES) ultrafiltration (UF) membrane with thermal stability and high fouling resistance using melamine-modified zirconium-based metal-organic framework (UiO-66-NH2/MOF). Sep Purif Technol 251:117010
Samari M et al (2021) A new fouling resistance polyethersulfone ultrafiltration membrane embedded by metformin-modified FSM-16: fabrication, characterization and performance evaluation in emulsified oil-water separation. J Environ Chem Eng 9(4):105386
Seman MA, Khayet M, Hilal N (2012) Comparison of two different UV-grafted nanofiltration membranes prepared for reduction of humic acid fouling using acrylic acid and N-vinylpyrrolidone. Desalination 287:19–29
Tavangar T et al (2020) Textile waste, dyes/inorganic salts separation of cerium oxide-loaded loose nanofiltration polyethersulfone membranes. Chem Eng J 385:123787
Vatanpour V et al (2012a) TiO2 embedded mixed matrix PES nanocomposite membranes: Influence of different sizes and types of nanoparticles on antifouling and performance. Desalination 292:19–29
Vatanpour V et al (2012b) Novel antibifouling nanofiltration polyethersulfone membrane fabricated from embedding TiO2 coated multiwalled carbon nanotubes. Sep Purif Technol 90:69–82
Vatanpour V et al (2012c) Boehmite nanoparticles as a new nanofiller for preparation of antifouling mixed matrix membranes. J Membr Sci 401:132–143
Vatanpour V et al (2020) Anti-fouling and permeable polyvinyl chloride nanofiltration membranes embedded by hydrophilic graphene quantum dots for dye wastewater treatment. J Water Process Eng 38:101652
Wang C et al (2018) Zwitterionic functionalized "cage-like" porous organic frameworks for nanofiltration membrane with high efficiency water transport channels and anti-fouling property. J Membr Sci 548:194–202
Xu C et al (2016) Preparation of PES ultrafiltration membranes with natural amino acids based zwitterionic antifouling surfaces. Appl Surf Sci 385:130–138
Yang Y et al (2012) Novel functionalized nano-TiO2 loading electrocatalytic membrane for oily wastewater treatment. Environ Sci Technol 46(12):6815–6821
Yao Y et al (2016) Development of a positively charged nanofiltration membrane for use in organic solvents. J Membr Sci 520:832–839
Zeng G et al (2016) Novel polyvinylidene fluoride nanofiltration membrane blended with functionalized halloysite nanotubes for dye and heavy metal ions removal. J Hazard Mater 317:60–72
Zhao H et al (2013) Improving the antifouling property of polysulfone ultrafiltration membrane by incorporation of isocyanate-treated graphene oxide. Phys Chem Chem Phys 15(23):9084–9092
Zinadini S et al (2014a) Preparation of a novel antifouling mixed matrix PES membrane by embedding graphene oxide nanoplates. J Membr Sci 453:292–301
Zinadini S et al (2014b) Novel high flux antifouling nanofiltration membranes for dye removal containing carboxymethyl chitosan coated Fe3O4 nanoparticles. Desalination 349:145–154
Zinadini S et al (2017) Preparation of antibiofouling polyethersulfone mixed matrix NF membrane using photocatalytic activity of ZnO/MWCNTs nanocomposite. J Membr Sci 529:133–141